



OPEN ACCESS

EDITED BY

Mohlopheni Jackson Marakalala,
Africa Health Research Institute (AHRI), South
Africa

REVIEWED BY

Dina R. Weillhammer,
Lawrence Livermore National Laboratory
(DOE), United States
Harjeet Singh,
Narnarayan Shastri Institute of Technology,
India
Kudakwashe Nyambo,
Stellenbosch University, South Africa

*CORRESPONDENCE

Pengtao Wang

✉ wangpengtao2021@163.com

Wei Jia

✉ jiawei202412@163.com

[†]These authors have contributed equally to
this work

RECEIVED 23 October 2025

REVISED 17 December 2025

ACCEPTED 30 December 2025

PUBLISHED 27 January 2026

CITATION

Li Q, Li S, Kang Y, Xue J, Wang P and Jia W
(2026) Metabolite analysis of *Aspergillus
fumigatus* conidial supernatant and its
pro-inflammatory activity *in vitro* and *in vivo*.
Front. Immunol. 16:1730825.
doi: 10.3389/fimmu.2025.1730825

COPYRIGHT

© 2026 Li, Li, Kang, Xue, Wang and Jia. This is
an open-access article distributed under the
terms of the [Creative Commons Attribution
License \(CC BY\)](https://creativecommons.org/licenses/by/4.0/). The use, distribution or
reproduction in other forums is permitted,
provided the original author(s) and the
copyright owner(s) are credited and that the
original publication in this journal is cited, in
accordance with accepted academic
practice. No use, distribution or reproduction
is permitted which does not comply with
these terms.

Metabolite analysis of *Aspergillus fumigatus* conidial supernatant and its pro-inflammatory activity *in vitro* and *in vivo*

Qiujie Li^{1†}, Shan Li^{1†}, Yuting Kang¹, Jian Xue²,
Pengtao Wang^{3*} and Wei Jia^{3,4*}

¹First Clinical Medical College, Ningxia Medical University, Yinchuan, China, ²Senior Department of Cardiology, The Sixth Medical Center of Chinese PLA General Hospital, Beijing, China, ³Ningxia Key Laboratory of Clinical and Pathogenic Microbiology, Institute of Medical Sciences, General Hospital of Ningxia Medical University, Yinchuan, China, ⁴Center of Medical Laboratory, General Hospital of Ningxia Medical University, Yinchuan, China

Introduction: *Aspergillus fumigatus* (*A. fumigatus*) conidia have been reported to induce inflammatory response in macrophages, resulting in lung damage. However, the role of secondary metabolites secreted by conidia during the infection process remains unclear. Our objective is to investigate the metabolic changes produced by conidia at different developmental stages and to assess the effects of the conidial supernatant on the inflammatory response of macrophages.

Methods: We employed optical microscopy, electron microscopy, and nuclear division staining to identify the morphological characteristics of the *Aspergillus fumigatus* strain Af293 conidia at various developmental stages. Metabolomic analysis of the supernatant from conidial pre-germination (Af293-4h) and post-germination (Af293-12h) was performed using Liquid Chromatography-Mass Spectrometry. Conidial supernatant was utilized to stimulate mouse alveolar macrophages (MH-S) cells, and the expression of inflammatory factors was quantified using ELISA and RT-qPCR. Western blotting was conducted to detect the levels of key proteins involved in the inflammatory pathway. Furthermore, mice were administered an intranasal instillation of the supernatant to construct the pneumonia model, and lung pathology was evaluated through hematoxylin-eosin (HE) staining, while the levels of inflammatory factors in bronchoalveolar lavage fluid were assessed using ELISA and RT-qPCR.

Results: Non-targeted metabolomics analyses reveal an increased secretion of organic acids and their derivatives, lipids and lipid-like molecules, phenolic compounds, phenylpropanoids, polyketides, as well as alkaloids and their derivatives following conidial germination. Compared to Af293-4h supernatant, Af293-12h supernatant induce a significantly stronger inflammatory response in MH-S cells, characterized by the increased expression of inflammatory factors, including IL-1 β , TNF- α , CCL/CXCL and MMPs, via the activation of JAK/STAT/AKT and MAPK signaling pathways. Nasal exposure of conidial supernatant in mice can induce lung inflammation, resulting in lung damage and an elevated proportion of inflammatory cells, as well as increased levels of the inflammatory factors such as TNF- α , IL-1 β , and IL-6.

Conclusion: Our research indicates significant differences in the metabolites of *A. fumigatus* conidial supernatant between the pre-germination and post-

germination stages. The conidial supernatant can induce a pronounced inflammatory response in macrophages, mediated by the activation of the JAK/STAT/MAPK pathways. Long-term exposure to spore supernatant in mice can result in pneumonia and tissue damage.

KEYWORDS

A. fumigatus, conidia, germination, inflammatory response, metabolite

1 Introduction

Aspergillus fumigatus (*A. fumigatus*) is a filamentous, airborne saprophytic fungus that contributes to elevated rates of pulmonary infections and mortality in humans, thus imposing a substantial burden on global health (1). *A. fumigatus* typically exists in the air as conidia, which are generally cleared by the mucociliary system and resident macrophages in healthy individuals (2–4). However, in immunocompromised patients, the lung tissue's ability to clear conidia is compromised, leading to increased adhesion and germination of *A. fumigatus*, which can result in invasive aspergillosis (IA) (5–7). Research has demonstrated that *A. fumigatus* conidia can induce inflammatory response in pulmonary epithelial cells and macrophages, causing a robust inflammatory reaction in immunocompetent mice and resulting in pathological damage to the lungs (8–10). Moreover, conidia possess various secretory substances, including multiple proteases, allergens, and toxins, and other secondary metabolites, to evade macrophage phagocytosis (11, 12). One such mycotoxin, gliotoxin, has been shown to disrupt the pulmonary epithelial barrier and promote immune evasion (13–15). It has been verified that conidial supernatant can damage the bronchial epithelial monolayer, exacerbating the clinical symptoms of cystic fibrosis (14). These findings indicate that, in addition to conidia, its secondary metabolites also exert a detrimental effect on lung tissue, warranting further investigation.

Macrophages are a crucial component of the innate immune system, playing a pivotal role in pathogen recognition, inflammation regulation, and tissue homeostasis. Traditionally, it has been believed that adult macrophages primarily originate from bone marrow monocytes; however, recent lineage-tracing and single-cell studies have demonstrated that many tissue-resident macrophages (TRMs) have an embryonic origin, deriving from yolk sac or fetal liver progenitors, and can be maintained long-term through local self-renewal (16, 17). Alveolar macrophages are representative of embryonically derived TRMs and primarily depend on self-renewal under steady-state conditions. During instances of infection or tissue injury, bone marrow-derived monocytes supplement and differentiate into inflammatory macrophages. Upon encountering fungal invasions, macrophages

can recognize fungi, activate host immunity, and eliminate conidia to inhibit fungal proliferation (18). Recent research has established that the dectin-1 receptor on alveolar macrophages can recognize β -glucans on the surface of fungal cells (19), thereby activating the MAPK signaling pathway to initiate the innate immune response of these macrophages (20). Furthermore, both mouse and human alveolar macrophages can phagocytose *A. fumigatus* conidia through mechanisms involving actin polymerization and phosphatidylinositol 3-kinase activation (21). It has also been found that the melanin present on the surface of conidia can modulate glucose and glutamine metabolism in macrophages, promoting cellular inflammation (22, 23). Research shows that after infection with *A. fumigatus*, various pro-inflammatory factors are elevated in macrophage cell line RAW264.7, including TNF- α , IL-1 β , IL-1 α , CXCL-1, CXCL-2, and GM-CSF, leading to an inflammatory response (8, 24). *A. fumigatus* conidia induces higher levels of cytokines TNF- α , IL-6, IL-1 β , and IL-18 in bone marrow-derived macrophages (25). *Aspergillus fumigatus* can induce pulmonary inflammatory responses in mice by promoting the expression of various inflammatory factors such as CXCL-2, IL-1 α , CXCL-1, GM-CSF, IL-1 β , IL-6, and MIP-1 α (8). However, the role of metabolites produced by *A. fumigatus* during the infection process in macrophages remains unclear and requires further elucidation.

In recent years, studies on the secondary metabolism of *A. fumigatus* have demonstrated that the metabolic processes of filamentous fungi are influenced by various conditions, including nitrogen sources, carbon sources, pH levels, temperature, and light (26). This metabolism is regulated at multiple levels, including transcriptional, epigenetic, and post-translational (27–29). As a result, the metabolic changes that occur during the germination of conidia are complex, leading to a diverse array of secondary metabolites. These metabolites play crucial roles in a variety of biological processes, such as heat resistance, cell wall composition and maintenance, fulfillment of nutritional requirements, interactions with the host immune system, and responses to stress (1). Notable secondary metabolites include gliotoxin, fumonisin, verruculogen, restrictocin, helvolic acid, and proteases, each playing distinct ecological roles in fungal defense, dissemination, and virulence, particularly during infections, thereby impacting host

cells (30). The elastase and collagenase secreted by *A. fumigatus* can degrade alveolar tissue and disrupt the integrity of the epithelial barrier (31). Gliotoxin has been extensively studied for its cytotoxic and immunosuppressive properties, which have been documented in previous reports (32–34). However, these toxins are secreted only after the conidia germinate into hyphae (approximately 24 hours) (35–37), while the metabolite components of the early stages of conidia (before 12 hours) and their effects on host cells remain poorly understood. Therefore, we analyzed the differentially expressed metabolites secreted by *A. fumigatus* during two early growth stages (conidia and hyphae) using mass spectrometry and preliminarily explored the inflammatory response of these metabolites on macrophages. Furthermore, we established an *in vivo* model by performing intranasal instillation of mice with conidial supernatant to assess its effects on inflammation.

2 Materials and methods

2.1 Maintenance, storage, and culture condition of *A. fumigatus* strain Af293

In this study, the *A. fumigatus* strain Af293 (ATCC MYA-4609) was generously provided by Prof. Liu Wei from Peking University First Hospital. The fungal isolate was cultured on Sabouraud dextrose agar (SDA) medium at 37°C for a period of 5 to 7 days. Subsequently, the culture was treated with a washed solution of 0.05% Tween 80, and the conidia of Af293 were gently scraped off using a disposable pipette to obtain a conidia suspension. This suspension was then stored at -80°C in the Medical Laboratory Center of the General Hospital of Ningxia Medical University for long-term preservation for future research applications.

2.2 Determination of Af293 conidial germination rate

The prepared conidial suspensions were inoculated into seven 50 mL centrifuge tubes, each containing 15 mL of Czapek medium, achieving a final concentration of 1×10^5 conidia/mL. The conidial concentration was quantified by diluting the prepared conidial suspension in a gradient from 1:10 to 1:1000 as necessary. The conidia were counted using a Neubauer counting chamber under an optical microscope. The conidial concentration was calculated using the formula (average count $\times 10^4 \times$ dilution factor), ensuring a final concentration of 1×10^5 conidia/mL. The tubes were incubated in a shaking incubator at 37°C and 200 rpm for durations of 0, 2, 4, 6, 8, 10, and 12 hours. At each time point, a small sample was placed on a microscope slide, covered with a coverslip, and examined under a standard optical microscope to observe the germination of 100–200 conidia. Germination was defined as a germ tube length that is greater than or equal to the conidia radius. The conidia germination rate was calculated using the formula: Germination rate (%) = $(a/A) \times 100$, where 'a' represents the number of germinated conidia (units) and 'A' denotes the total number of conidia observed (units).

2.3 Observation of Af293 conidia germination morphology

For optical microscopy, samples collected from the seven time points described in Section 2.2 were placed on slides, covered with coverslips, and observed under a standard optical microscope at 40 \times magnification, with photographic documentation accompanying the observations. For scanning electron microscopy (SEM), samples from the seven time points outlined in Section 2 were washed 1–2 times with phosphate-buffered saline (PBS), fixed in 3% glutaraldehyde, and subsequently rinsed three times with ultrapure water for 10 minutes each. The samples were then fixed with 1% osmium tetroxide for 1–2 hours, followed by three additional rinses with ultrapure water (10 minutes each), and dehydrated stepwise with ethanol at concentrations of 30%, 50%, 70%, 90%, and 100% (15 minutes per step at 100% concentration). A drop of the sample was placed on a coverslip and dried in a critical point dryer. Finally, the coverslip was attached to the sample stage using conductive adhesive and placed in an ion sputter coater for gold coating. Image acquisition was performed using a JEOL JSM-IT700HR scanning electron microscope.

2.4 Cell nuclear division staining of Af293 conidia

Samples from the seven time points in Step 2.2 were washed 1–2 times with PBS, followed by fixation at room temperature for 2 hours using a 2.5% glutaraldehyde solution. After fixation, the samples were washed again 1–2 times with PBS and stained with a DAPI working solution at room temperature for 20 minutes. Subsequently, the samples were washed once more with PBS, prepared as slides, mounted, and observed under a fluorescence microscope for photographic documentation.

2.5 Maintenance of murine alveolar macrophages (MH-S) cell lines

In this study, MH-S were cultured in RPMI 1640 growth medium supplemented with 10% fetal bovine serum (FBS) and 1% penicillin-streptomycin. They were maintained under controlled conditions of 5% CO₂ at 37°C. MH-S cells were periodically subcultured and used during the exponential growth phase for the experiments.

2.6 Treatment of MH-S cells with supernatant from Af293 conidia

Af293 conidia were cultured in SDA medium at a concentration of 1×10^5 conidia/mL for durations of 4 hours and 12 hours, respectively. The supernatant were collected and passed through a sterile cell sieve, followed by sterile filtration using a 0.22 μ m syringe filter (Merck Millipore) to eliminate all conidia and hyphae,

achieving a final concentration of 100%. Subsequently, cells were stimulated with the supernatant from both 4-hour and 12-hour cultures to obtain a 1% concentration of supernatant in complete medium.

2.7 Conidial supernatant induced lung inflammation in the mouse model

The animal experiments were approved by the Institutional Animal Ethics Research Board of the General Hospital of Ningxia Medical University (KYL-2024-0344). A total of 10 male BALB/c mice, aged 4 to 6 weeks and weighing between 18 and 20 grams, were obtained from Cloud-Clone Corp. The mice were housed in ventilated racks within the animal facility, with ad libitum access to food and water, and maintained on a 12-hour light/dark cycle. After a week of acclimatization, the mice were randomly divided into two equal groups: the Control (CTRL) group and the Conidial Supernatant-induced Lung Inflammation (CSLI) group. Mice in the CSLI group received a single intranasal instillation of 1% conidial supernatant (CS) of Af293-12h, diluted with phosphate-buffered saline (PBS), twice daily for one month, while the control group received PBS twice daily for the same duration.

2.8 Histopathological examination

To collect bronchoalveolar lavage fluid (BALF) samples, the mice were first anesthetized, and their tracheas were surgically exposed. Subsequently, the left lungs were washed twice with 2 ml of cold phosphate-buffered saline (PBS). Following this, BALF was centrifuged at 12,000×g for 10 minutes at 4°C, and the supernatant was collected for cytokine analysis using ELISA kits. The pellet was immediately processed for cell sorting, with white blood cells classified via Wright-Giemsa staining kit (G1079, Servicebio, China). For the right lungs, tissue samples were collected, fixed in 4% paraformaldehyde, embedded in paraffin, sectioned to a thickness of 5 μm, and stained using the HE Staining Kit (G1120, Solarbio, China).

2.9 RNA extraction and cytokine gene expression

Total RNA was extracted from conidia, MH-S lung macrophages and lung tissue following the manufacturer's instructions using TRIzol reagent (Thermo Scientific, Rockford, IL, USA). The total RNA was reverse-transcribed into cDNA using a first-strand cDNA synthesis kit (TaKaRa, Shiga, Japan), in accordance with the manufacturer's guidelines. The resulting cDNA was amplified with the primers listed in Table 1. The PCR amplification conditions were as follows: an initial cycle at 95°C for 30 seconds, followed by 45 cycles at 95°C for 5 seconds and 60°C for

TABLE 1 Sequences of primers used in the study.

Genes	Primers	Sequences
<i>A. fumigatus</i>		
<i>Rho</i>	Sense	5'-GACTACGTCCACCACCTACAG-3'
	Antisense	5'-GGCTAGCATCTCCAGTCAGAG-3'
<i>RasA</i>	Sense	5'-GATTGAGAGTCACTTCGTCG-3'
	Antisense	5'-CTAAGACATCCAACAAGCG-3'
<i>RacA</i>	Sense	5'-GGGACTGTGGGATACTGCTG-3'
	Antisense	5'-GCTCAATCTCCGGGTACCAC-3'
<i>GAPDH</i>	Sense	5'-GCCTCTTAAGGGTATCCTGACCTA-3'
	Antisense	5'-TACCAGCTCACCAACTTCACGA-3'
Mouse		
IL-1β	Sense	5'-TGGACCTTCCAGGATGAGGACA-3'
	Antisense	5'-GTTTCATCTCGGAGCCTGTAGTG-3'
IL-6	Sense	5'-CTTGCAAGACTTCCATCCAC-3'
	Antisense	5'-AGTGGTAGACAGGTCTGTTGC-3'
TNF-α	Sense	5'-CCTGTAGCCCACGTCGTAC-3'
	Antisense	5'-GGGAGTAGACAAGGTACAACCC-3'
CCL-2	Sense	5'-CTCAGCCAGATGCAGTTAACG-3'
	Antisense	5'-CAGACCTCTCTCTTGAGCTTGG-3'
CCL-7	Sense	5'-GCTGCTTTCAGCATCCAAGTG-3'
	Antisense	5'-CCAGGGACACCGACTACTG-3'
CXCL-2	Sense	5'-GTTGACTTCAAGAATCCAG-3'
	Antisense	5'-CTTCTCTCTTGGTTCTCCG-3'
CXCL-3	Sense	5'-ATCCCAACGGTGTCTGGATG-3'
	Antisense	5'-GCAAGTAGATGCAATTATACCCGT-3'
MMP9	Sense	5'-GCCCTGGAAGTACACGACA-3'
	Antisense	5'-TTGGAAGTACACGCCAGAAG-3'
MMP13	Sense	5'-GATGGACCTTCTGGTCTTCT-3'
	Antisense	5'-GCTCATGGGACGCAACAATA-3'
GAPDH	Sense	5'-GGTGTCTCTGCGACTTCA-3'
	Antisense	5'-TGGTCCAGCGTTTCTTACTCC-3'

30 seconds, concluding with a final cycle at 95°C for 5 seconds, 60°C for 60 seconds, and 95°C for 15 seconds. The relative levels of target genes were calculated and normalized to GAPDH levels, with all experiments conducted in triplicate. mRNA expression levels were determined using the Livak method ($2^{-\Delta\Delta CT}$).

2.10 Enzyme-linked immunosorbent assay

To evaluate the concentrations of TNF-α, IL-1β, and IL-6 in either the cell culture medium or the bronchoalveolar lavage fluid (BALF) obtained from mouse models of CSLI, cytokine levels were measured using ELISA kits according to the manufacturer's instructions. The specific kits used were JL10484-96T for TNF-α, JL18442-96T for IL-1β, and JL20268-96T for IL-6, all provided by J&L Biological Industrial, Shanghai, China. Each sample was analyzed in duplicate.

2.11 Protein extraction and Western blotting

MH-S lung macrophages were stimulated with a 1% concentration of supernatant derived from Af293 conidia during the 12-hour germ tube elongation phase (Af293-12h) for durations of 6 and 12 hours. The harvested MH-S cells were washed with ice-cold PBS and subsequently lysed using RIPA lysis solution (KGB5303, KeyGEN BioTECH, China), which contained protease and phosphatase inhibitors. Following extraction, the protein content of each sample was quantified using the BCA protein assay kit (KGB2101, KeyGEN BioTECH, China). Cellular proteins were then separated by electrophoresis on 10% SDS-PAGE gels and transferred to polyvinylidene fluoride (PVDF) membranes (Durapore[®] Millipore). The membranes were blocked in 5% skim milk in TBST for 1 hour at room temperature and then incubated with the primary antibody overnight at 4°C. The proteins of interest included AKT, JAK1, STAT1, JNK, ERK, as well as their phosphorylated forms: AKT, JAK1, STAT1, JNK (Thr183/Tyr185), and ERK (Thr202/Tyr204), along with GAPDH as a loading control. After washing the membranes with TBST, they were incubated with either horseradish peroxidase (HRP)-conjugated polyclonal goat anti-mouse or HRP-conjugated polyclonal goat anti-rabbit antibodies for 1 hour at room temperature, followed by three washes with TBST. Subsequently, the ECL reagent (Abbkine) was applied to the membranes, and luminescence imaging was performed using a Bio-Rad ChemiDoc imaging system. The density of each band was compared with the corresponding control band and normalized against GAPDH using densitometry with ImageJ software (version 2.3.0). Results are expressed as a percentage of the untreated control.

2.12 Metabolomic analysis of *Aspergillus fumigatus* supernatant

This study analyzed metabolites using an ACQUITY UPLC I-Class Plus ultra-high-performance liquid chromatography-tandem mass spectrometry system, coupled with a QE Plus high-resolution mass spectrometer and relevant databases including METLIN, Lipidmaps, ChEBI (38–41). Samples were collected from two groups: pre-germination (4-hour swelling phase) and post-germination (12-hour germ tube elongation phase), with six biological replicates per group, resulting in a total of 12 samples. A 1 mL sample was extracted using the solid-phase extraction (SPE) column, followed by the collection of 3 mL of methanol eluent. The sample underwent nitrogen blowdown using a nitrogen evaporator. After drying under nitrogen, 300 μ L of pre-chilled methanol-water (V:V = 4:1, containing a mixed internal standard at 4 μ g/mL) was added and vortexed for one minute. The mixture was subjected to ultrasonic treatment in an ice-water bath for 10 minutes and then allowed to stand overnight at -40°C. Subsequently, it was centrifuged for 10 minutes at 12,000 rpm and 4°C. A total of 150 μ L of the supernatant was drawn using a syringe, filtered through a 0.22 μ m organic phase syringe filter, and transferred to an

LC injection vial. The samples were stored at -80°C until LC-MS analysis. Mass spectrometry was performed in both positive and negative ion modes. The raw LC-MS data underwent baseline filtering, peak identification, integration, retention time correction, peak alignment, and normalization, facilitated by Progenesis QI V2.3 software (Nonlinear Dynamics, Newcastle, UK). Principal Component Analysis (PCA) was employed to visualize the overall distribution among samples and to assess analytical stability throughout the process. Orthogonal Partial Least Squares Discriminant Analysis (OPLS-DA) and Partial Least Squares Discriminant Analysis (PLS-DA) were utilized to distinguish metabolite differences between the groups. Variable Importance Projection (VIP) values derived from the OPLS-DA model ranked each variable's overall contribution to group discrimination. Bilateral Student's t-tests were subsequently applied to validate the statistical significance of inter-group metabolite differences. Differential metabolites with VIP values exceeding 1.0 and p-values below 0.05 were selected and annotated for metabolic pathways via the Kyoto Encyclopedia of Genes and Genomes (KEGG) database (42), identifying the metabolic pathways in which these differential metabolites participated.

2.13 Statistical analysis

Statistical analysis was conducted using GraphPad Prism 10.0 (La Jolla, USA). Data are presented as mean \pm standard deviation (SD) and were analyzed using the unpaired Student's t-test for two groups or one-way analysis of variance (ANOVA) with Dunnett's *post hoc* test for three or more groups, followed by the Bonferroni *post hoc* test. A p-value of less than 0.05 was considered indicative of significant differences.

3 Results

3.1 Morphological characteristics of Af293 conidial germination

To observe the morphological characteristics during the early germination process of Af293 conidia, we selected a culture duration of 0 to 12 hours, employing optical microscopy, DAPI staining, and scanning electron microscopy. The results indicated that the conidia began to swell significantly at 4 hours, with a small number initiating germination at 6 hours, and the majority completing germination after 12 hours, as observed both under the optical microscope and in test tubes (Figures 1A, B). Consequently, we propose that the conidia undergo a water absorption and swelling phase from 0 to 4 hours, a polar growth phase from 4 to 8 hours, and a germ tube growth phase from 8 to 12 hours. DAPI staining revealed that changes in nuclear division occurred during the water absorption and swelling phase, with an increase in the number of nuclei during the polar growth phase (Figure 1C). The germination rate also significantly increased

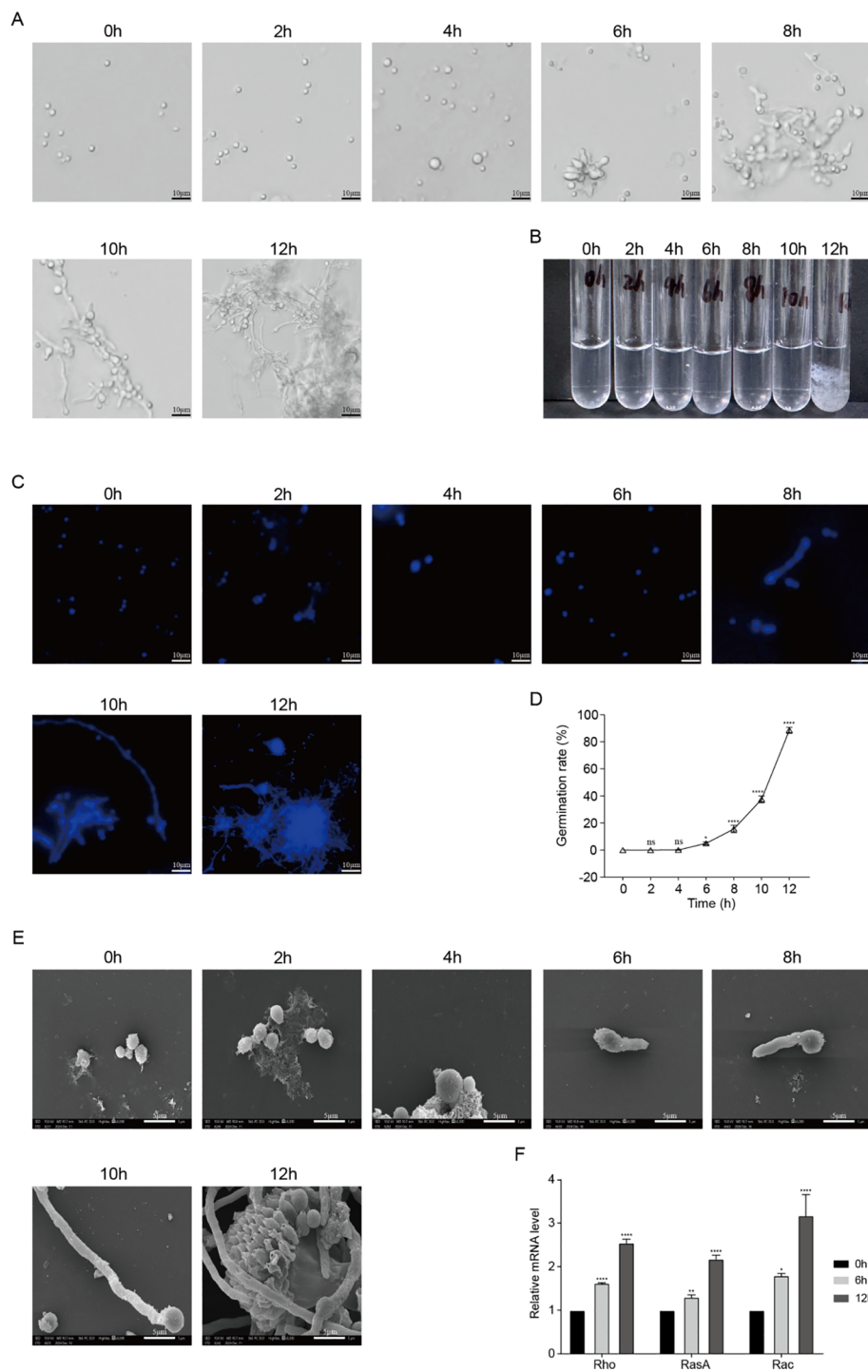


FIGURE 1

Morphological characteristics of conidial germination of *A. fumigatus* Af293. **(A)** Morphological observations of *A. fumigatus* at different germination times under an optical microscope (scale bar = 10 μ m); **(B)** Morphological observations of Af293 at different germination times in culture media; **(C)** DAPI staining of conidia with different morphologies (scale bar = 5 μ m); **(D)** Germination rates of Af293 conidia at various time points; **(E)** Morphological observations of Af293 at different germination times under a scanning electron microscope (scale bar = 5 μ m); **(F)** Relative mRNA levels of polar growth-related genes *Rho*, *RasA*, and *Rac* as determined by RT-qPCR. (* p < 0.05, ** p < 0.01, *** p < 0.001, **** p < 0.001 in one-way ANOVA with Tukey's multiple comparison).

between 6 and 12 hours (Figure 1D), which aligns with the results obtained from electron microscopy (Figure 1E). We selected three time points: pre-germination (0h), polar growth phase (6h), and germ tube growth phase (12h), and measured the mRNA expression

levels of polar growth-related genes during the germination process using RT-qPCR. We found that, compared to 0h, the mRNA levels of *Rho*, *RasA*, and *Rac* were significantly elevated at 6h and 12h (Figure 1F). These results indicate that Af293 conidia exhibit

distinct morphological characteristics at various germination stages and demonstrate a clear time-dependent relationship.

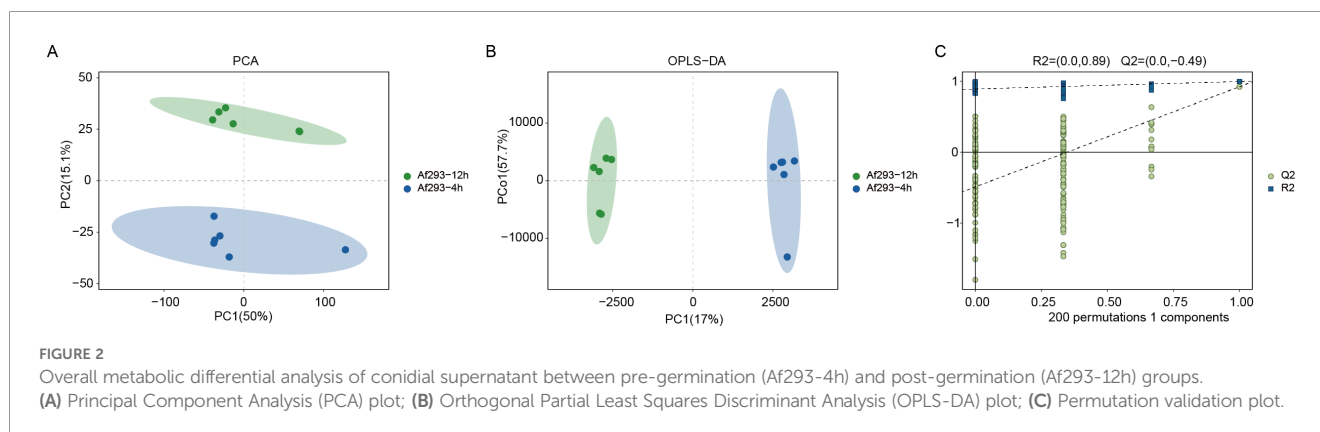
3.2 Overall sample differential analysis of conidial supernatant

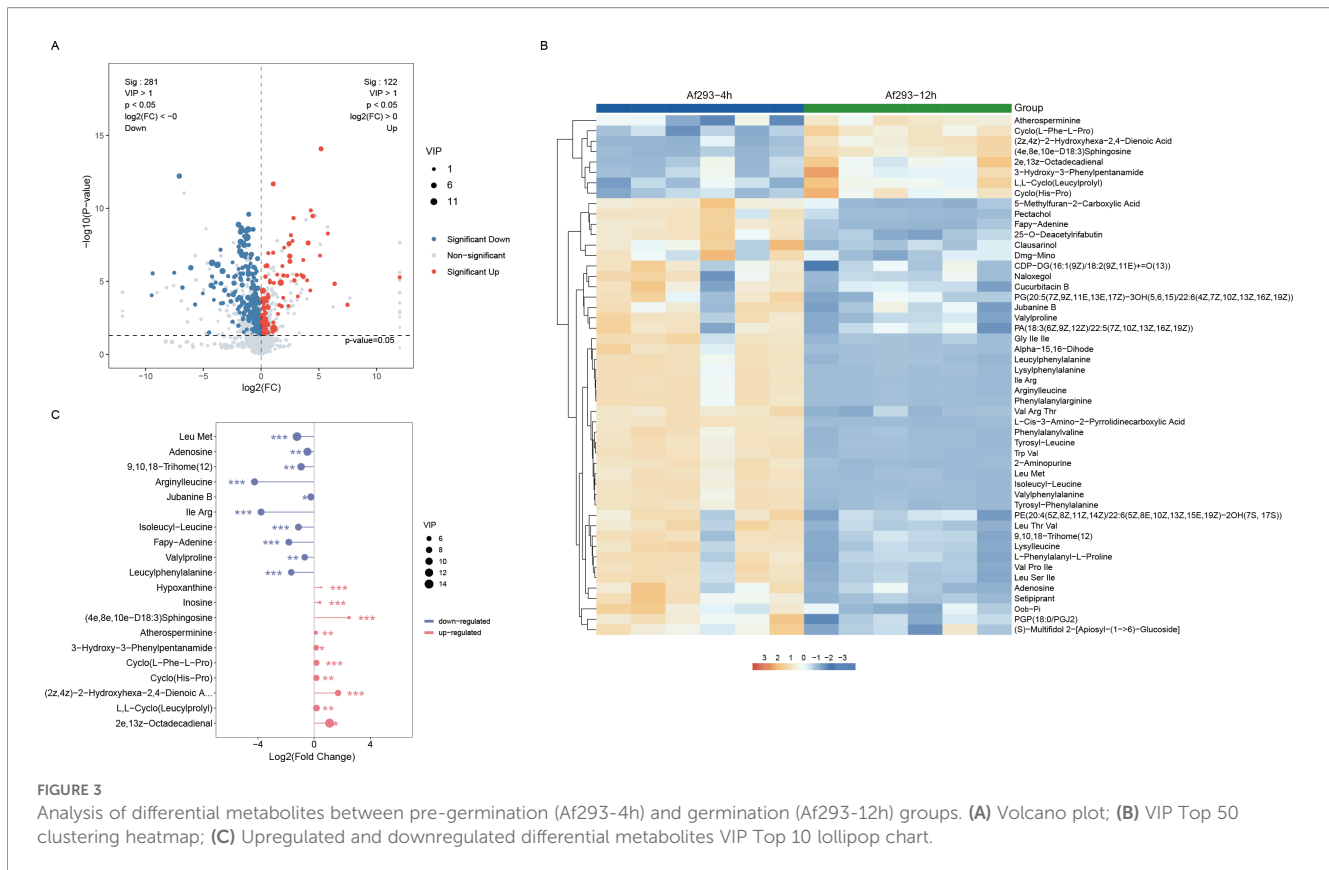
Previous results have demonstrated significant morphological differences in the conidia of Af293 between the pre-germination and germination stages, indicating potential metabolic variations in the secreted metabolites during these phases. In our study, the 4-hour point (Af293-4h) corresponds to the pre-germination and early swelling phase, during which conidia have absorbed water, initiated isotropic growth, and begun transcriptional activation, yet have not produced a visible germ tube. In contrast, the 12-hour point (Af293-12h) represents the post-germination and early hyphal outgrowth phase, characterized by the establishment of polarized growth and a marked reprogramming of primary metabolism. Therefore, we employed mass spectrometry to analyze the metabolic differences in the conidial supernatant between the pre-germination (Af293-4h) and post-germination (Af293-12h) stages. The results of the Principal Component Analysis (PCA) revealed that the first principal component accounted for 50% of the variance, while the second principal component accounted for 15.1%. The relative distances among points within each sample group were notably small and tightly distributed, indicating a concentrated distribution; however, a significant trend of separation between the groups was observed (Figure 2A). To further investigate the differences in metabolites, we employed Orthogonal Partial Least Squares Discriminant Analysis (OPLS-DA) to eliminate irrelevant data variations, thereby enhancing the capture of differential metabolite information between the two groups. We observed significant differences between the two sample groups in the OPLS-DA score plot (Figure 2B). Additionally, we performed a permutation test with 200 iterations on the model, randomly permuting the variables of the previously defined classification Y matrix (e.g., 0 or 1) n times ($n=200$) to establish corresponding OPLS-DA models and obtain the R^2 and Q^2 values of the random models. As illustrated in Figure 2C, $R^2 = 0.89$ exceeds $Q^2 = -0.49$, and the Q^2 regression line

intercept with the Y-axis is less than 0, indicating that the model possesses reasonable predictive capability. The model demonstrates robust explanatory power for the samples, accurately reflecting the information contained within them (Figure 2C).

3.3 Differential metabolite analysis of conidial supernatant

Based on the OPLS-DA model, the variable importance in projection (VIP) values for each metabolite were obtained, with a general consensus that metabolites with $VIP > 1$ are statistically significant. The results from the volcano plot indicate that in the Af293-12h group, 40 metabolites are upregulated and 101 metabolites are downregulated compared to the Af293-4h group, adhering to the screening criteria of p -value < 0.05 , fold change (FC) > 2 or $FC < 0.5$, and $VIP > 1$ (Figure 3A). These metabolites primarily consist of organic acids and their derivatives, lipids and lipid-like molecules, as well as organic heterocyclic compounds. We performed hierarchical clustering on all significantly different metabolites based on the expression levels of the top 50 VIP values; the hierarchical clustering heatmap clearly illustrates significant differences in metabolite abundance between the two sample groups. Compared to the Af293-4h group, the abundances of Atherosperminine, Cyclo(L-Phe-L-Pro), (2z,4z)-2-Hydroxyhexa-2,4-Dienoic Acid, (4e,8e,10e)-D18:3 Sphingosine, 2e,13z-Octadecadienal, 3-Hydroxy-3-Phenylpentanamide, L,L-Cyclo(Leucylprolyl), and Cyclo(His-Pro) significantly increased in the Af293-12h group. In contrast, the abundances of 5-Methylfuran-2-Carboxylic Acid, Pectachol, Fapy-Adenine, and 42 other metabolites markedly decreased in the Af293-12h group (Figure 3B). We presented the top ten differential metabolites with the highest VIP values in Figure 3C and Table 2. Compared to the Af293-4h group, the metabolites that exhibited a decrease in the Af293-12h group include Leu Met, adenosine, 9,10,18-Trihome (12), arginylleucine, jubanine B, Ile Arg, isoleucyl-leucine, fapy-adenine, valylproline, and leucylphenylalanine. In addition to the eight significantly elevated metabolites indicated in the heatmap, both Hypoxanthine and Inosine also demonstrated increased levels in the Af293-12h group.





3.4 KEGG pathway enrichment analysis of differential metabolites

KEGG enrichment analysis was performed to explore the relationships between the differential metabolites and metabolic pathways. As illustrated in Figure 4, the top 20 pathways with the lowest p -values during the germination period (Af293-12h), in comparison to the water absorption swelling period (Af293-4h), are presented. The upregulated pathways that were significantly enriched include linoleic acid metabolism, lysine degradation, and tryptophan metabolism ($p < 0.05$) (Figure 4A). Conversely, the downregulated pathways are primarily enriched in linoleic acid metabolism, ABC transporters, the biosynthesis of phenylalanine, tyrosine, and tryptophan, astaxanthin biosynthesis, aminoacyl-tRNA biosynthesis, the biosynthesis of various secondary metabolites, and purine metabolism ($p < 0.05$) (Figure 4B).

3.5 Inflammatory response in MH-S cells induced by conidial supernatant

Although *A. fumigatus* conidia can elicit an inflammatory response in macrophages, the effects of conidial supernatant over varying time periods on macrophage inflammatory response remain unclear. We treated MH-S cells with supernatant from Af293 at 4 hours and 12 hours, subsequently assessing the expression of inflammatory factors using ELISA and RT-qPCR.

The ELISA results indicated that both the Af293-4h and Af293-12h groups induced the expression of inflammatory factors IL-1 β and TNF- α , with levels in the Af293-12h group significantly higher than those in the Af293-4h group (Figure 5A). The RT-qPCR results revealed that levels of IL factors, including IL-1 β and TNF- α , chemokines such as CCL-2, CCL-7, CXCL-2, and CXCL-3, as well as metalloproteinases including MMP-9 and MMP-13, were all elevated in the Af293-12h group compared to the Af293-4h group (Figure 5B). This indicates that the supernatant from germinated Af293 can induce a stronger inflammatory response.

3.6 Conidial supernatant induced inflammation through the activation of JAK-STAT and MAPK pathways

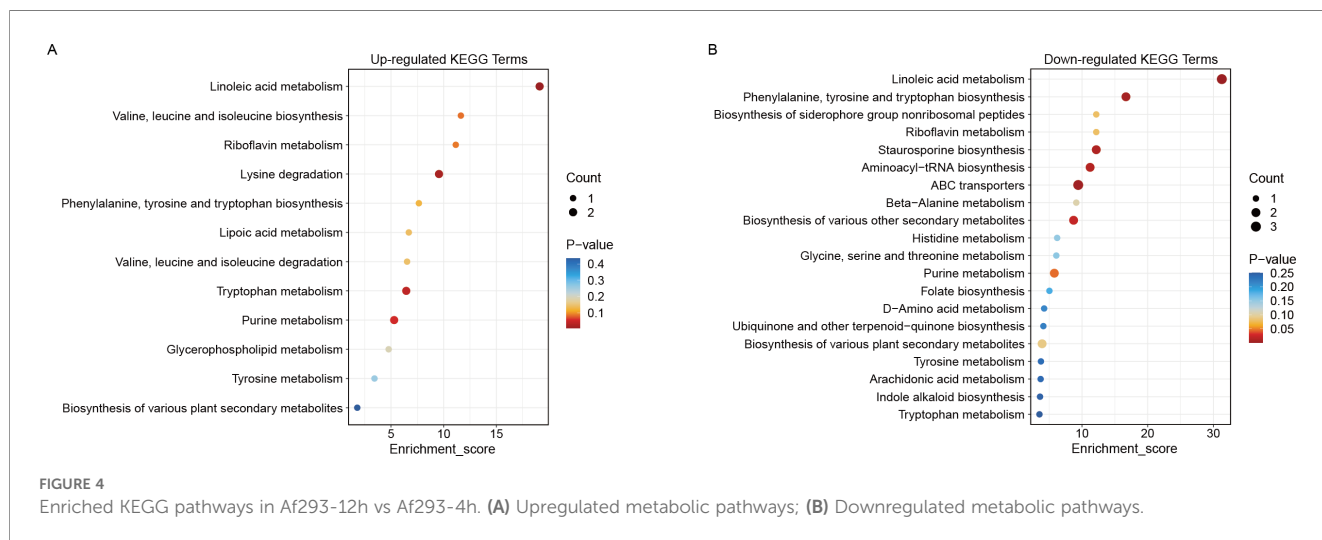
Infection with *A. fumigatus* can activate various inflammatory pathways, including the JAK-STAT (43, 44) and MAPK (20, 45) pathways, which have not been previously reported to be induced by the conidial supernatant. To investigate this, we stimulated MH-S cells with the Conidial Supernatant (CS) from Af293-12h, as it is known to induce a more robust inflammatory response. We then assessed the overall protein levels and phosphorylation states of key proteins involved in inflammatory signaling pathways, including JAK1, STAT1, AKT, JNK, and ERK, using Western blot (WB) analysis. The results indicated that the phosphorylation levels of these proteins were significantly elevated after 12 hours of CS treatment, suggesting the activation of these pathways

TABLE 2 Top 10 Metabolites with up-regulated and down-regulated differences.

Metabolites	Retention time (min)	Formula	Mass-to-charge ratio (m/z)
Leu Met	3.850766666666667	C11H22N2O3S	263.139784717201
Adenosine	1.171883333333333	C10H13N5O4	312.09551943557
9,10,18-Trihome (12)	7.123766666666667	C18H34O5	329.233850316604
Arginylleucine	1.314533333333333	C12H25N5O3	288.203028787236
Jubanine B	4.640616666666667	C43H47N5O6	730.360110195805
Ile Arg	1.155866666666667	C12H25N5O3	288.203092939169
Isoleucyl-Leucine	3.974016666666667	C12H24N2O3	245.186438320647
Fapy-Adenine	0.751833333333333	C5H7N5O	136.062203943373
Valylproline	1.815633333333333	C10H18N2O3	215.13936196682
Leucylphenylalanine	4.506466666666667	C15H22N2O3	279.170572830627
Hypoxanthine	1.301383333333333	C5H4N4O	137.046106610468
Inosine	1.28685	C10H12N4O5	269.088312408884
(4e, 8e, 10e-D18:3) Sphingosine	10.669533333333333	C18H33NO2	296.258778971969
Atherosperminine	4.3397	C20H23NO2	327.206689275614
3-Hydroxy-3-Phenylpentanamide	4.611116666666667	C11H15NO2	211.144513581141
Cyclo(L-Phe-L-Pro)	4.94325	C14H16N2O2	245.128782644162
Cyclo(His-Pro)	0.7632	C11H14N4O2	235.119638001593
(2z, 4z)-2-Hydroxyhexa-2,4-Dienoic Acid	1.975266666666667	C6H8O3	111.04465425608
L, L-Cyclo(Leucylprolyl)	4.746383333333333	C11H18N2O2	211.144443254875
2e,13z-Octadecadienal	12.6619	C18H32O	282.279423603985

(Figures 6A, B). To elucidate the signaling pathways activated by CS that lead to inflammatory responses, we employed the AKT inhibitor (AZD5363, 50uM) and the phosphorylated-ERK inhibitor (PD98059, 50uM) to inhibit the relevant pathway proteins and evaluate the alterations in downstream inflammatory factors. Figure 6C shows that AZD5363 and PD98059 effectively inhibited the expression of AKT and phosphorylated-ERK,

respectively. As illustrated in Figure 6D, both AZD5363 and PD98059 significantly reduced the elevated concentrations of the inflammatory factors IL-1 β and TNF- α induced by CS. The RT-qPCR results (Figure 6E) indicated that AZD5363 significantly decreased the mRNA levels of the inflammatory factors IL-1 β , TNF- α , CCL-2, CXCL-2, and MMP9, while PD98059 resulted in a reduction of the mRNA levels of IL-1 β , CXCL-2, MMP9, and



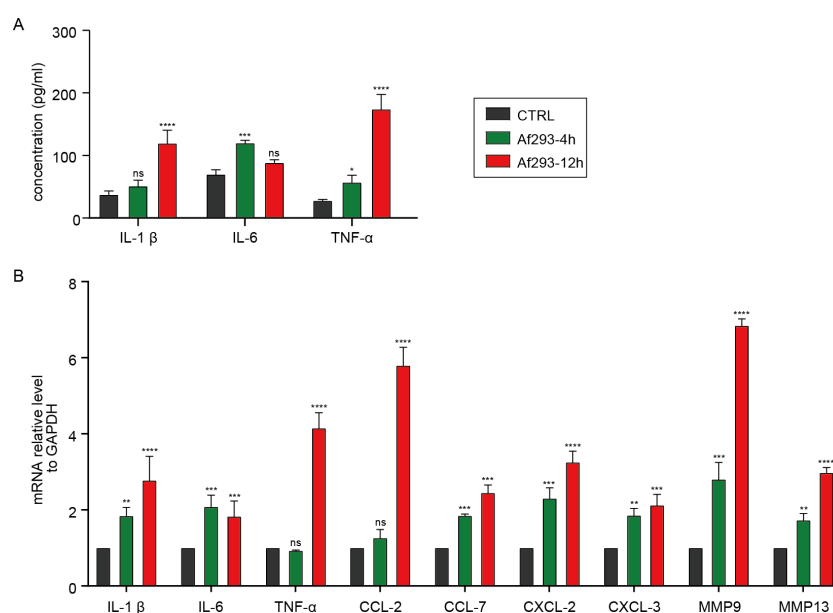


FIGURE 5

Levels of inflammatory factors in MH-S cells treated with supernatant from Af293 at 4 hours (Af293-4h) and 12 hours (Af293-12h). (A) The concentration of inflammatory factors in the cell supernatant was detected using ELISA; (B) The mRNA levels of inflammatory factors within the cells were assessed through RT-QPCR. (* $p < 0.05$, ** $p < 0.01$, *** $p < 0.001$, **** $p < 0.0001$ in one-way ANOVA with Tukey's multiple comparison).

MMP13. These findings imply that CS-12h promotes the phosphorylation of multiple inflammatory-related proteins, thereby stimulating MH-S cells to produce elevated levels of inflammatory factors and response.

3.7 Conidial supernatant induced lung inflammation in mice

Conidial supernatant has the capacity to stimulate inflammation in MH-S cells; however, its potential to induce lung inflammation *in vivo* remains unclear. To address this issue, we established a mouse pneumonia model by continuously administering conidial supernatant via intranasal instillation for one month, referred to as the CLSI group. The control group received intranasal instillation of PBS. Hematoxylin and eosin (HE) staining revealed inflammatory cell infiltration and pulmonary emphysema in the lung tissue of mice in the CLSI group, indicating damage to lung tissue caused by conidial supernatant (Figure 7A). Cytological analysis using Giemsa staining demonstrated a marked increase in macrophages and neutrophils, along with a slight but statistically non-significant increase in lymphocytes in the bronchoalveolar lavage fluid (BALF) of mice in the CLSI group compared to the control group (Figure 7B). At the molecular level, ELISA results showed significantly elevated levels of pro-inflammatory cytokines (TNF- α , IL-1 β , and IL-6) in the BALF of mice in the CLSI group (Figure 7C). This finding was corroborated by RT-qPCR analysis of inflammatory markers in lung tissue (Figure 7D). In summary, we have established a mouse model of chronic pneumonia induced by conidial supernatant, which provides a reliable platform for the

in-depth investigation of host interactions with Af293 conidial supernatant.

4 Discussion

This study systematically elucidates, for the first time, the dynamic relationship between the conidia germination process of *A. fumigatus* and its pathogenicity. As conidia germinate, *A. fumigatus* undergoes significant metabolic reprogramming, accompanied by toxin accumulation. Non-targeted metabolomics analysis reveals an increased secretion of organic acids and derivatives, lipids and lipid-like molecules, phenolic compounds, phenylpropanoids, polyketides, as well as alkaloids and their derivatives following conidia germination. Moreover, the metabolic characteristics of its secretome and its capacity to induce host inflammatory response are dynamic, markedly intensifying over time. Compared to pre-germination supernatant, those from the post-germination supernatant induce significantly stronger inflammatory response *in vitro*. These secondary metabolites activate host inflammatory response *in vitro* via the JAK/STAT/AKT and MAPK pathways. Thus, studying the inflammatory response mediated by conidial supernatant serves as a crucial complement to the mechanisms of conidia infection. This approach provides significant insights into the comprehensive understanding of the pathogenic process of *A. fumigatus*.

Our morphological observations indicate that the conidia transition from a dormant to an active germination state between 4 and 12 hours. These two time points encapsulate the primary differences in metabolic states before and after germination,

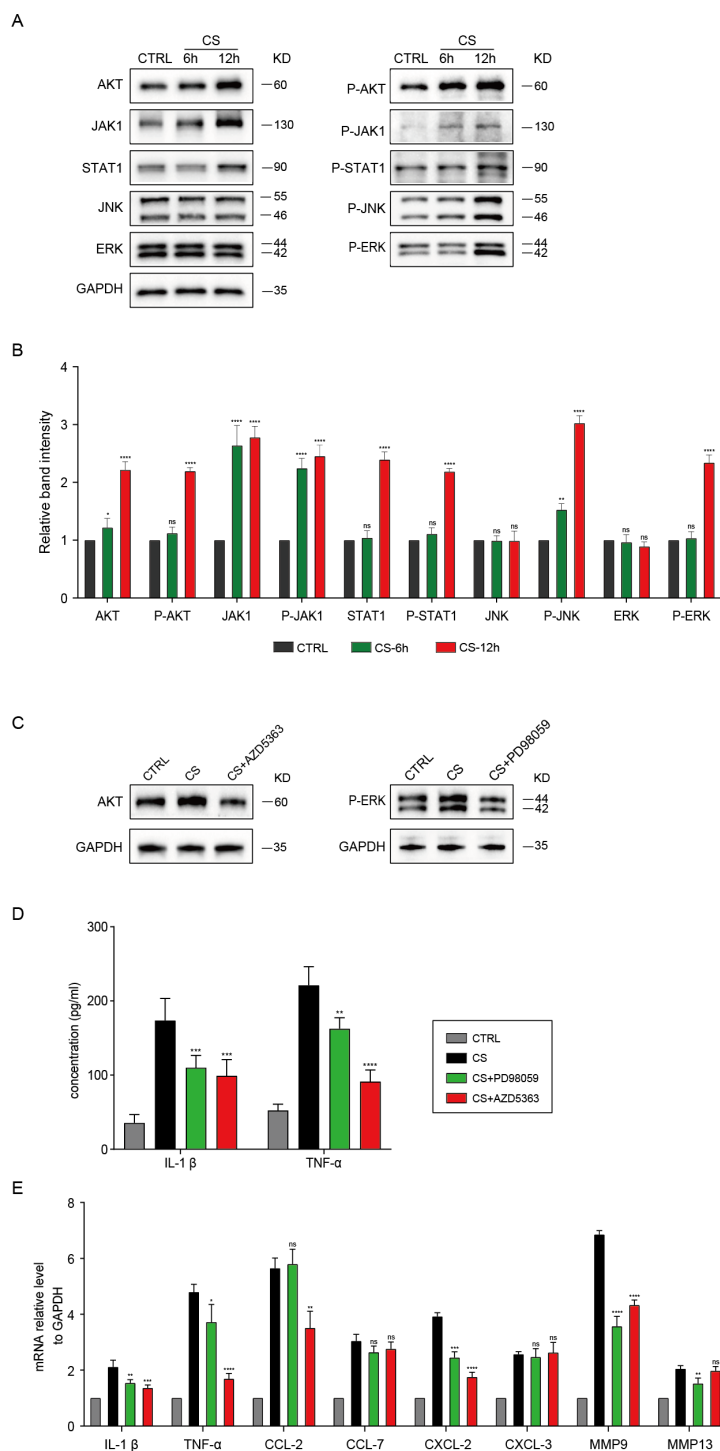
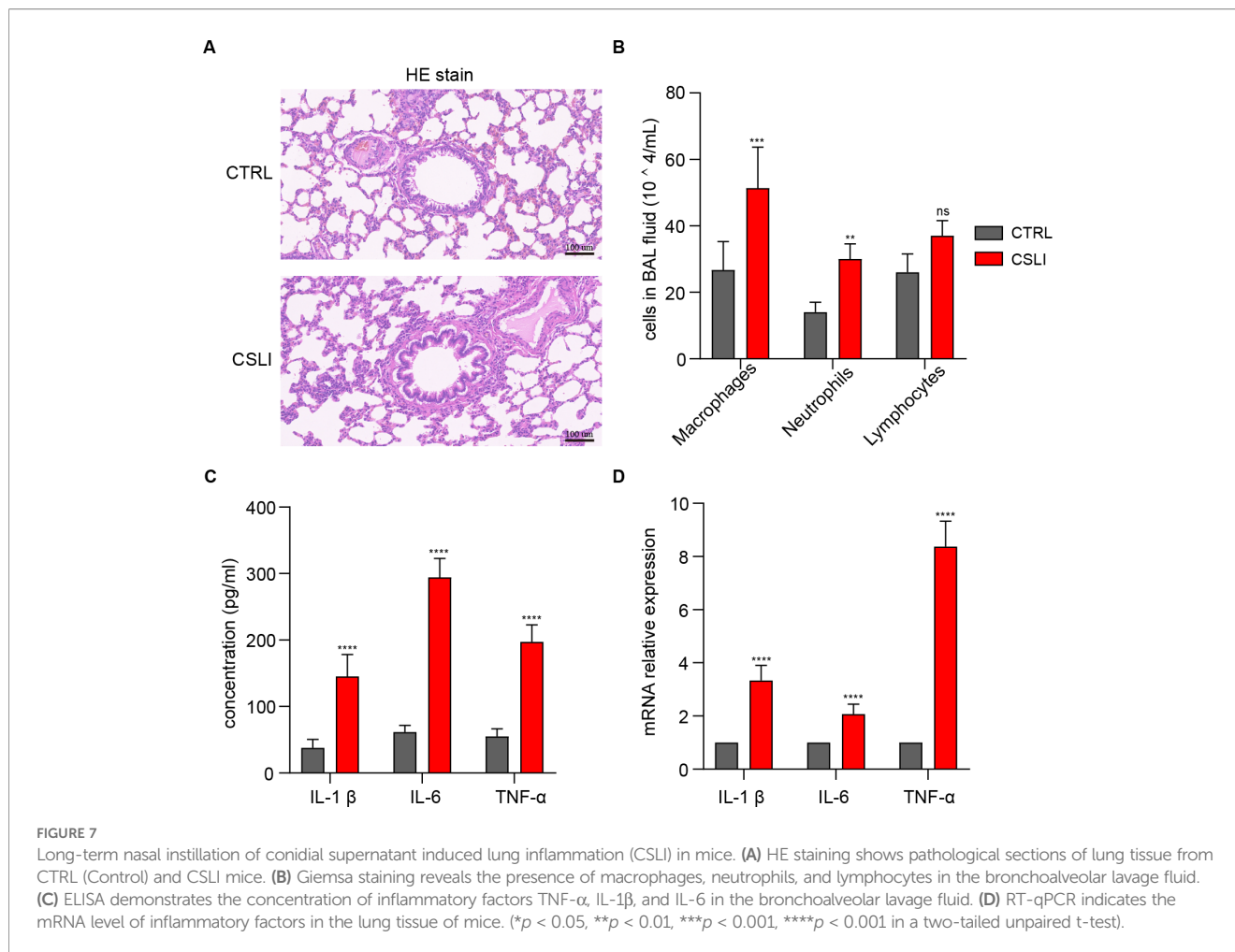


FIGURE 6

The total protein and phosphorylation levels of the JAK-STAT and MAPK pathways in MH-S cells treated with Conidial Supernatant (CS) were assessed at 6 and 12 hours. **(A)** The total levels of proteins and phosphorylated proteins involved in the JAK-STAT and MAPK pathways were assessed using Western blotting. **(B)** The relative band intensity from Figure 6A was quantified. **(C)** The inhibitory effects of the AKT inhibitor (AZD5363, 50uM) and the phosphorylated-ERK inhibitor (PD98059, 50uM) on phosphorylated-ERK were assessed using Western blotting. **(D)** The concentration of inflammatory factors in treated cells with inhibitors AZD5363 or PD98059 were measured using ELISA. **E:** The mRNA levels of inflammatory factors in cells treated with the inhibitors AZD5363 or PD98059 were measured using RT-qPCR. (* $p < 0.05$, ** $p < 0.01$, *** $p < 0.001$, **** $p < 0.001$ in one-way ANOVA with Tukey's multiple comparison).



facilitating the identification of key metabolites and pathway alterations associated with the initiation of germination. Consistent with this observation, mass spectrometry analysis revealed significant differences in the metabolites present in the supernatant at these two time points. Overall, the tryptophan metabolic pathway in *A. fumigatus* is markedly upregulated. Existing literature confirms that *A. fumigatus* produces multiple tryptophan-containing toxins, including fumigaclavine C, fumiquinazoline C, fumitremorgin, gliotoxin, and hexadecydroastechrome (46). The synthesis of these toxins depends on tryptophan, which provides essential structural components (47). Given that humans and other mammals cannot synthesize tryptophan, the ability of *A. fumigatus* to autonomously produce this amino acid enables it to sustain growth and continuously synthesize toxins in nutritionally limited environments, such as the lungs of hosts. This metabolic advantage enables the fungus to dominate during infection without relying on tryptophan supplied by the host (48). On the other hand, our results indicate a significantly upregulated linoleic acid metabolic pathway during the germination of *A. fumigatus*. This finding is corroborated by other studies that demonstrate *A. fumigatus* metabolizes linoleic acid through specific oxidase systems, such as lipoxygenases (49). Furthermore, studies have

confirmed that 5,8-diHODE, an endogenously produced and secreted dihydroxyoxylipin, regulates the differentiation process of filamentous fungi, including lateral branching in pathogenic *A. fumigatus* and *Aspergillus flavus* (50). These findings suggest that germinating conidia do not passively release substances; rather, they actively undergo 'metabolic reprogramming,' potentially altering the nature of their interactions with the host immune system. However, we must acknowledge that selecting only two time points (4 hours and 12 hours) for metabolite detection is insufficient. Consequently, future studies will incorporate additional time points for metabolite detection during conidia growth.

Functional assays confirmed the biological consequences of these metabolic alterations. We first demonstrated that the conidial supernatant of Af293-12h induced a greater release of inflammatory cytokines in cellular models compared to the conidial supernatant of Af293-4h. We hypothesize that the enhanced pro-inflammatory capacity of the CS-12h may arise from the accumulation of certain metabolites, such as diketopiperazine compounds, including L, L-Cyclo (Leucylprolyl), Cyclo (L-Phe-L-Pro), and Cyclo (His-Pro). Notably, Cyclo(L-Phe-L-Pro) has been previously reported (51). These can be regarded as core skeletons or direct biosynthetic precursors of gliotoxin and its related

mycotoxins. The elevated metabolite (2Z,4Z)-2-hydroxyhexa-2,4-dienoic acid may serve as a key intermediate or degradation product in the biosynthetic pathway of polyketides, based on its chemical structure. Certain metabolites, such as hypoxanthine and inosine, which exhibit marked increases, may play a role in the adaptive survival and sustained growth of *A. fumigatus*. For *A. fumigatus*, sphingosine is essential for maintaining cell wall integrity and toxicity (52, 53). Sphingolipid signaling is critical for the formation of fungal biofilms, which are vital for persistent infection and drug resistance (54, 55). Among these differential metabolites, it is necessary to conduct further experiments to confirm which specific metabolites are responsible for the inflammatory response.

Inflammation triggered by *A. fumigatus* conidia infection is characterized as a “biphasic” process. The initial phase of inflammation is primarily initiated by the physical interaction between pathogen-associated molecular patterns (PAMPs) present on the conidia surface and host pattern recognition receptors, such as Dectin-1 and Toll-like receptors (TLRs), leading to rapid and intense signaling (19, 22). The later phase, which coincides with conidia germination and hyphal formation, is marked by the continuous secretion of effectors, including toxins and proteases, which persistently intensify and amplify the inflammatory response, potentially resulting in more severe damage to host cells. Previous studies have indicated that *A. fumigatus* conidia can stimulate host cells and activate the phosphorylation of the PI3K/AKT, JAK/STAT, and MAPK pathways (44, 56, 57). Our findings reveal that the conidial supernatant stimulation leads to elevated levels of inflammatory protein phosphorylation in cells, including PI3K/AKT, JAK/STAT, and MAPK pathways. Furthermore, the inhibition of ERK and AKT resulted in a significant decrease in the inflammatory factors IL-1 β , TNF- α , and CXCL-2. A study conducted by Xiao Cui et al. demonstrated that *A. fumigatus* conidia can activate the MAPK signaling pathway in BEAS-2B epithelial cells, resulting in the induction of cytokine production (58). Notably, the application of a JNK inhibitor reversed the secretion of inflammatory factors induced by *A. fumigatus* in BEAS-2B cells, whereas inhibitors of p38 MAPK and ERK did not influence these processes. This discrepancy may stem from the differences in MAPK pathways between epithelial cells and macrophages. In a separate study (59), exposure of BEAS-2B cells to *A. fumigatus* conidia activated the AKT/mTOR pathway, leading to cellular inflammation and apoptosis. Furthermore, *A. fumigatus* conidia stimulated the release of cytokines from dendritic cells, promoting Th17 responses, including IL-1 β , IL-6, and IL-23, via the JAK/STAT signaling pathway (44). These studies indicate that conidia or conidial supernatant can promote inflammatory responses by activating various signaling pathways. *Aspergillus*-mediated allergic airway inflammation was confirmed through repeated intranasal exposure to *A. fumigatus* conidia (A1160) in mouse model (60). Another study revealed that immunocompetent mice subjected to *A. fumigatus* conidia (AFsp group) exhibited a pronounced inflammatory response, characterized by an increase in

the number of bronchoalveolar lavage fluid (BALF) macrophages and elevated expression of inflammatory factors (IL-1 β , CXCL-2, CXCL-1, GM-CSF, IL-6), which are associated with lung injury (8). These findings align with our established pneumonia model in immunocompetent mice, developed through nasal instillation of *A. fumigatus* conidial supernatant over one month. Consequently, prolonged nasal exposure to conidial supernatant or conidia induces similar pulmonary inflammation in the mice.

However, this study has several limitations. First, the supernatant represents a complex mixture of components. Although we have identified key metabolites through correlation analysis, further research is necessary for metabolite quantification and to ascertain which metabolites play significant roles in the inflammatory response. Second, it is essential to validate pneumonia induced by the supernatant of *A. fumigatus* in a larger cohort of mice. The duration and frequency of exposure to supernatant stimulation must be repeated and confirmed, and additional pathological analyses of pneumonia in mice should be conducted. Third, although the conidial supernatant cannot form colonies on PDA plates, the possibility of residual protein components that may induce inflammatory responses cannot be excluded. Therefore, we need to assess the purity of the supernatant through controls, including proteinase K treatment or heat inactivation, and we will subsequently reevaluate the inflammatory effects in future studies.

5 Conclusion

Our research indicates significant differences in the metabolites of *A. fumigatus* conidial supernatant between the pre-germination and post-germination stages. The conidial supernatant can induce a pronounced inflammatory response in macrophages, mediated by the activation of the JAK/STAT/MAPK pathways. Long-term exposure to spore supernatant in mice can result in pneumonia and tissue damage. Therefore, the development of preventive or intervention strategies targeting these specific metabolites or the inflammatory pathways they activate presents significant potential.

Data availability statement

The data presented in the study are deposited in the OMIX repository, China National Center for Bioinformation/Beijing Institute of Genomics, Chinese Academy of Sciences, accession number OMIX010709.

Ethics statement

The animal study was approved by Institutional Animal Ethics Research Board of the General Hospital of Ningxia Medical University (KYLL-2024-0344). The study was conducted in accordance with the local legislation and institutional requirements.

Author contributions

QL: Formal Analysis, Writing – original draft, Data curation, Methodology, Conceptualization, Investigation. SL: Formal Analysis, Writing – original draft, Methodology, Investigation, Conceptualization. YK: Methodology, Writing – original draft. JX: Writing – original draft, Software. PW: Writing – original draft, Data curation, Investigation. WJ: Supervision, Conceptualization, Validation, Writing – review & editing.

Funding

The author(s) declared that financial support was received for this work and/or its publication. This work was supported by the Natural Science Foundation of Ningxia Hui Autonomous Region (grant no. 2025AAC030983).

Acknowledgments

We would like to thank Shanghai Luming Biological Technology Co., Ltd. (Shanghai, China) for providing the metabolomics services.

References

- Earle K, Valero C, Conn DP, Vere G, Cook PC, Bromley MJ, et al. Pathogenicity and virulence of *Aspergillus fumigatus*. *Virulence*. (2023) 14:2172264. doi: 10.1080/21505594.2023.2172264
- Denning DW, O'Driscoll BR, Hogaboam CM, Bowyer P, Niven RM. The link between fungi and severe asthma: a summary of the evidence. *Eur Respir J*. (2006) 27:615–26. doi: 10.1183/09031936.06.00074705
- Black PN, Udy AA, Brodie SM. Sensitivity to fungal allergens is a risk factor for life-threatening asthma. *Allergy*. (2000) 55:501–4. doi: 10.1034/j.1398-9995.2000.00293.x
- Goh KJ, Yii ACA, Lapperre TS, Chan AK, Chew FT, Chotirmall SH, et al. Sensitization to *Aspergillus* species is associated with frequent exacerbations in severe asthma. *J Asthma Allergy*. (2017) 10:131–40. doi: 10.2147/JAA.S130459
- Speirs JJ, van der Ent CK, Beekman JM. Effects of *Aspergillus fumigatus* colonization on lung function in cystic fibrosis. *Curr Opin Pulm Med*. (2012) 18:632–8. doi: 10.1097/MCP.0b013e328358d50b
- Agarwal R, Muthu V, Sehgal IS, Dhooria S, Prasad KT, Aggarwal AN. Allergic bronchopulmonary aspergillosis. *Clin Chest Med*. (2022) 43:99–125. doi: 10.1016/j.ccm.2021.12.002
- Perfect JR. The impact of the host on fungal infections. *Am J Med*. (2012) 125:S39–51. doi: 10.1016/j.amjmed.2011.10.010
- Bouyssi A, Déméautis T, Trecourt A, Delles M, Agostini F, Monneret G, et al. Characterization of lung inflammatory response to *Aspergillus fumigatus* spores. *J Fungi (Basel)*. (2023) 9:682. doi: 10.3390/jof9060682
- Smith NL, Denning DW. Underlying conditions in chronic pulmonary aspergillosis including simple aspergilloma. *Eur Respir J*. (2010) 37:865–72. doi: 10.1183/09031936.00054810
- Lauruschkat CD, Etter S, Schnack E, Ebel F, Schäuble S, Page L, et al. Chronic occupational mold exposure drives expansion of aspergillus-reactive type 1 and type 2 T-helper cell responses. *J Fungi (Basel)*. (2021) 7:698. doi: 10.3390/jof7090698
- Adav SS, Ravindran A, Sze SK. Quantitative proteomic study of *Aspergillus fumigatus* secretome revealed deamidation of secretory enzymes. *J Proteomics*. (2015) 119:154–68. doi: 10.1016/j.jprot.2015.02.007

Conflict of interest

The author(s) declared that this work was conducted in the absence of any commercial or financial relationships that could be construed as a potential conflict of interest.

Generative AI statement

The author(s) declared that generative AI was not used in the creation of this manuscript.

Any alternative text (alt text) provided alongside figures in this article has been generated by Frontiers with the support of artificial intelligence and reasonable efforts have been made to ensure accuracy, including review by the authors wherever possible. If you identify any issues, please contact us.

Publisher's note

All claims expressed in this article are solely those of the authors and do not necessarily represent those of their affiliated organizations, or those of the publisher, the editors and the reviewers. Any product that may be evaluated in this article, or claim that may be made by its manufacturer, is not guaranteed or endorsed by the publisher.

- Ben-Ami R, Lewis RE, Kontoyiannis DP. Enemy of the (immunosuppressed) state: an update on the pathogenesis of *Aspergillus fumigatus* infection. *Br J Haematol*. (2010) 150:406–17. doi: 10.1111/j.1365-2141.2010.08283.x
- Crossen AJ, Ward RA, Reedy JL, Surve MV, Klein BS, Rajagopal J, et al. Human airway epithelium responses to invasive fungal infections: A critical partner in innate immunity. *J Fungi (Basel)*. (2022) 9:40. doi: 10.3390/jof9010040
- Dunne K, Reece E, McClean S, Doyle S, Rogers TR, Murphy P, et al. *Aspergillus fumigatus* supernatants disrupt bronchial epithelial monolayers: potential role for enhanced invasion in cystic fibrosis. *J Fungi (Basel)*. (2023) 9:490. doi: 10.3390/jof9040490
- Coméra C, André K, Laffitte J, Collet X, Galtier P, Maridonneau-Parini I. Gliotoxin from *Aspergillus fumigatus* affects phagocytosis and the organization of the actin cytoskeleton by distinct signalling pathways in human neutrophils. *Microbes Infect*. (2006) 9:47–54. doi: 10.1016/j.micinf.2006.10.009
- Wu Y, Hirschi KK. Tissue-resident macrophage development and function. *Front Cell Dev Biol*. (2021) 8:617879. doi: 10.3389/fcell.2020.617879
- Wang Z, Wu Z, Wang H, Feng R, Wang G, Li M, et al. An immune cell atlas reveals the dynamics of human macrophage specification during prenatal development. *Cell*. (2023) 186:4454–71. doi: 10.1016/j.cell.2023.08.019
- Xu S, Shinohara ML. Tissue-resident macrophages in fungal infections. *Front Immunol*. (2017) 8:1798. doi: 10.3389/fimmu.2017.01798
- Quäschling T, Friedrich D, Deepe GS, Rupp J. Crosstalk between autophagy and hypoxia-inducible factor-1 α in antifungal immunity. *Cells*. (2020) 9:2150. doi: 10.3390/cells9102150
- Dubourdeau M, Athman R, Balloy V, Huerre M, Chignard M, Philpott DJ, et al. *Aspergillus fumigatus* induces innate immune responses in alveolar macrophages through the MAPK pathway independently of TLR2 and TLR4. *J Immunol*. (2006) 177:3994–4001. doi: 10.4049/jimmunol.177.6.3994
- Ibrahim-Granet O, Philippe B, Boleti H, Boisvieux-Ulrich E, Grenet D, Stern M, et al. Phagocytosis and intracellular fate of *Aspergillus fumigatus* conidia in alveolar macrophages. *Infect Immun*. (2003) 71:891–903. doi: 10.1128/IAI.71.2.891-903.2003

22. Antunes D, Gonçalves SM, Matzaraki V, Rodrigues CS, Gonçalves RA, Rocha J, et al. Glutamine Metabolism Supports the Functional Activity of Immune Cells against *Aspergillus fumigatus*. *Microbiol Spectr.* (2022) 11:e0225622. doi: 10.1128/spectrum.02256-22
23. Gonçalves SM, Duarte-Oliveira C, Campos CF, Aimaniana V, Ter Horst R, Leite L, et al. Phagosomal removal of fungal melanin reprograms macrophage metabolism to promote antifungal immunity. *Nat Commun.* (2020) 11:2282. doi: 10.1038/s41467-020-16120-z
24. Luan J, Zhu Y, Lin J, Zhang Y, Xu Q, Zhan L, et al. Quercetin protects against *Aspergillus fumigatus* keratitis by reducing fungal load and inhibiting TLR-4 induced inflammatory response. *Cytokine.* (2023) 171:156356. doi: 10.1016/j.cyto.2023.156356
25. Pinzan CF, Valero C, de Castro PA, da Silva JL, Earle K, Liu H, et al. *Aspergillus fumigatus* conidial surface-associated proteome reveals factors for fungal evasion and host immunity modulation. *Nat Microbiol.* (2024) 9:2710–26. doi: 10.1038/s41564-024-01782-y
26. Lind AL, Smith TD, Saterlee T, Calvo AM, Rokas A. Regulation of secondary metabolism by the velvet complex is temperature-responsive in *Aspergillus*. *G3 (Bethesda).* (2016) 6:4023–33. doi: 10.1534/g3.116.033084
27. Moon H, Han K-H, Yu J-H. Upstream regulation of development and secondary metabolism in *Aspergillus* species. *Cells.* (2022) 12:2. doi: 10.3390/cells12010002
28. Keller NP. Fungal secondary metabolism: regulation, function and drug discovery. *Nat Rev Microbiol.* (2019) 17:167–80. doi: 10.1038/s41579-018-0121-1
29. Tudzynski B. Nitrogen regulation of fungal secondary metabolism in fungi. *Front Microbiol.* (2014) 5:656. doi: 10.3389/fmicb.2014.00656
30. Latgé J-P, Chamilos G. *Aspergillus fumigatus* and aspergillosis in 2019. *Clin Microbiol Rev.* (2019) 33:e00140-18. doi: 10.1128/CMR.00140-18
31. Stergiopoulou T, Meletiadis J, Roilides E, Kleiner DE, Schaufele R, Roden M, et al. Host-dependent patterns of tissue injury in invasive pulmonary aspergillosis. *Am J Clin Pathol.* (2007) 127:349–55. doi: 10.1309/UJRV9DLC11RM3G8R
32. Scharf DH, Heinekamp T, Remme N, Hortschansky P, Brakhage AA, Hertweck C. Biosynthesis and function of gliotoxin in *Aspergillus fumigatus*. *Appl Microbiol Biotechnol.* (2011) 93:467–72. doi: 10.1007/s00253-011-3689-1
33. Zhang C, Chen F, Liu X, Han X, Hu Y, Su X, et al. Gliotoxin induces coflin phosphorylation to promote actin cytoskeleton dynamics and internalization of *Aspergillus fumigatus* into type II human pneumocyte cells. *Front Microbiol.* (2019) 10:1345. doi: 10.3389/fmicb.2019.01345
34. Arias M, Santiago L, Vidal-García M, Redrado S, Lanuza P, Comas L, et al. Preparations for invasion: modulation of host lung immunity during pulmonary aspergillosis by gliotoxin and other fungal secondary metabolites. *Front Immunol.* (2018) 9:2549. doi: 10.3389/fimmu.2018.02549
35. Lewis RE, Wiederhold NP, Lionakis MS, Prince RA, Kontoyiannis DP. Frequency and species distribution of gliotoxin-producing *Aspergillus* isolates recovered from patients at a tertiary-care cancer center. *J Clin Microbiol.* (2005) 43:6120–2. doi: 10.1128/JCM.43.12.6120-6122.2005
36. Guruceaga X, Perez-Cuesta U, Pellon A, Cendon-Sanchez S, Pelegri-Martinez E, Gonzalez O, et al. *Aspergillus fumigatus* fumagillin contributes to host cell damage. *J Fungi (Basel).* (2021) 7:936. doi: 10.3390/jof7110936
37. Illek B, Fischer H, Machen TE, Hari G, Clemons KV, Sass G, et al. Protective role of CFTR during fungal infection of cystic fibrosis bronchial epithelial cells with *Aspergillus fumigatus*. *Front Cell Infect Microbiol.* (2023) 13:1196581. doi: 10.3389/fcimb.2023.1196581
38. Smith CA, O'Maille G, Want EJ, Qin C, Trauger SA, Brandon TR, et al. METLIN: a metabolite mass spectral database. *Ther Drug Monit.* (2005) 27:747–51. doi: 10.1097/01.ftd.0000179845.53213.39
39. Guijas C, Montenegro-Burke JR, Domingo-Almenara X, Palermo A, Warth B, Hermann G, et al. METLIN: A technology platform for identifying knowns and unknowns. *Anal Chem.* (2018) 90:3156–64. doi: 10.1021/acs.analchem.7b04424
40. Sud M, Fahy E, Cotter D, Brown A, Dennis EA, Glass CK, et al. LMSD: LIPID MAPS structure database. *Nucleic Acids Res.* (2006) 35:D527–32. doi: 10.1093/nar/gkl838
41. Degtyarenko K, de Matos P, Ennis M, Hastings J, Zbinden M, McNaught A, et al. ChEBI: a database and ontology for chemical entities of biological interest. *Nucleic Acids Res.* (2007) 36:D344–50. doi: 10.1093/nar/gkm791
42. Okuda S, Yamada T, Hamajima M, Itoh M, Katayama T, Bork P, et al. KEGG Atlas mapping for global analysis of metabolic pathways. *Nucleic Acids Res.* (2008) 36:W423–6. doi: 10.1093/nar/gkn282
43. Chen F, Zhang C, Jia X, Wang S, Wang J, Chen Y, et al. Transcriptome profiles of human lung epithelial cells A549 interacting with *Aspergillus fumigatus* by RNA-seq. *PLoS One.* (2015) 10:e0135720. doi: 10.1371/journal.pone.0135720
44. Han F, Guo H, Wang L, Zhang Y, Sun L, Dai C, et al. TSLP produced by *Aspergillus fumigatus*-stimulated DCs promotes a Th17 response through the JAK/STAT signaling pathway in fungal keratitis. *Invest Ophthalmol Vis Sci.* (2020) 61:24. doi: 10.1167/iov.61.14.24
45. Briard B, Karki R, Malireddi RKS, Bhattacharya A, Place DE, Mavuluri J, et al. Fungal ligands released by innate immune effectors promote inflammasome activation during *Aspergillus fumigatus* infection. *Nat Microbiol.* (2018) 4:316–27. doi: 10.1038/s41564-018-0298-0
46. Choera T, Zelante T, Romani L, Keller NP. A multifaceted role of tryptophan metabolism and indoleamine 2,3-dioxygenase activity in *Aspergillus fumigatus*-host interactions. *Front Immunol.* (2018) 8:1996. doi: 10.3389/fimmu.2017.01996
47. Acerbi E, Hortova-Kohoutkova M, Choera T, Keller N, Fric J, Stella F, et al. Modeling approaches reveal new regulatory networks in *Aspergillus fumigatus* metabolism. *J Fungi (Basel).* (2020) 6:108. doi: 10.3390/jof6030108
48. Zelante T, Choera T, Beauvais A, Fallarino F, Paolicelli G, Pieraccini G, et al. *Aspergillus fumigatus* tryptophan metabolic route differently affects host immunity. *Cell Rep.* (2021) 34:108673. doi: 10.1016/j.celrep.2020.108673
49. Fischer GJ, Bacon W, Yang J, Palmer JM, Dagenais T, Hammock BD, et al. Lipoygenase activity accelerates programmed spore germination in *Aspergillus fumigatus*. *Front Microbiol.* (2017) 8:831. doi: 10.3389/fmicb.2017.00831
50. Niu M, Steffan BN, Fischer GJ, Venkatesh N, Raffa NL, Wettstein MA, et al. Fungal oxylipins direct programmed developmental switches in filamentous fungi. *Nat Commun.* (2020) 11:5158. doi: 10.1038/s41467-020-18999-0
51. Ibrahim SRM, Mohamed HM, Aljahdali AS, Murshid SSA, Mohamed SGA, Abdallah HM, et al. *Aspergillus fumigatus* from pathogenic fungus to unexplored natural treasure: changing the concept. *J Microbiol Biotechnol.* (2025) 35:e2411082. doi: 10.4014/jmb.2411.1082
52. Singh A, Del Poeta M. Lipid signalling in pathogenic fungi. *Cell Microbiol.* (2010) 13:177–85. doi: 10.1111/j.1462-5822.2010.01550.x
53. Shea JM, Del Poeta M. Lipid signaling in pathogenic fungi. *Curr Opin Microbiol.* (2006) 9:352–8. doi: 10.1016/j.mib.2006.06.003
54. Fabri JHTM, Rocha MC, Malavazi I. Overview of the interplay between cell wall integrity signaling pathways and membrane lipid biosynthesis in fungi: perspectives for *Aspergillus fumigatus*. *Curr Protein Pept Sci.* (2020) 21:265–83. doi: 10.2174/1389203720666190705164203
55. Zhai P, Song J, Gao L, Lu L. A sphingolipid synthesis-related protein OrmA in *Aspergillus fumigatus* is responsible for azole susceptibility and virulence. *Cell Microbiol.* (2019) 21:e13092. doi: 10.1111/cmi.13092
56. Yu B, Wang Q, Zhang L, Lin J, Feng Z, Wang Z, et al. Ebselen improves fungal keratitis through exerting anti-inflammation, anti-oxidative stress, and antifungal effects. *Redox Biol.* (2024) 73:103206. doi: 10.1016/j.redox.2024.103206
57. Yin M, Li C, Zhang L, Zhang L, Lin J, Jiang N, et al. Mechanism of antifungal activity and therapeutic action of β -ionone on *Aspergillus fumigatus* keratitis via suppressing LOX1 and JNK/p38 MAPK activation. *Int Immunopharmacol.* (2022) 110:108992. doi: 10.1016/j.intimp.2022.108992
58. Cui X, Chen F, Zhao J, Li D, Hu M, Chen X, et al. Involvement of JNK signaling in *Aspergillus fumigatus*-induced inflammatory factors release in bronchial epithelial cells. *Sci Rep.* (2023) 13:1293. doi: 10.1038/s41598-023-28567-3
59. Wang S, Gong L, Mo Y, Zhang J, Jiang Z, Tian Z, et al. Resveratrol attenuates inflammation and apoptosis through alleviating endoplasmic reticulum stress via Akt/mTOR pathway in fungus-induced allergic airways inflammation. *Int Immunopharmacol.* (2021) 103:108489. doi: 10.1016/j.intimp.2021.108489
60. Houlder EL, Gago S, Vere G, Furlong-Silva J, Conn D, Hickey E, et al. *Aspergillus*-mediated allergic airway inflammation is triggered by dendritic cell recognition of a defined spore morphotype. *J Allergy Clin Immunol.* (2024) 155:988–1001. doi: 10.1016/j.jaci.2024.10.040